A Coherent Processing Technique with High Precision for BDS B1I and B1C Signals

Yang Gao[1,2], Zheng Yao[1,2(✉)], and Mingquan Lu[1,2]

[1] Department of Electronic Engineering, Tsinghua University, Beijing, China
yaozheng@tsinghua.edu.cn
[2] Beijing National Research Center for Information Science and Technology, Beijing, China

Abstract. The smooth transition constraint and constant envelope restriction of the Beidou Navigation Satellite System (BDS) make the legacy regional system B1I signal and new global system B1C signal, which are located at different center frequencies, coexist in the BDS-3 B1 band. Therefore, new modulation and multiplexing techniques need to be adopted to meet these system constraints. More specifically, single-sideband complex binary offset carrier (SCBOC) modulation and constant envelope multiplexing via intermodulation construction (CEMIC) techniques are used in B1 band to construct a multicarrier constant-envelope composite navigation signal. In particular, the SCBOC modulation technique is introduced into the B1I signal to move its main energy from the global system B1 frequency to the regional system B1 frequency. However, as of now, the SCBOC modulation has only been regarded as a means to achieve the smooth update of the BDS, whose high-precision ranging potential has not been fully understood and utilized. To solve this problem, this paper proposes a high-precision coherent processing technique, which makes full use of the coherence between B1I and B1C signals. The proposed algorithm can not only exploit the ranging performance brought by high-frequency complex subcarriers without loss, but also greatly simplify the implementation complexity of the receiver. The experimental results of live BDS-3 signals verify the effectiveness and correctness of the proposed method. This paper provides a new solution for the high-precision application of the BDS B1 composite signal and has great reference value for receiver designers.

Keywords: BOC signal · Complex subcarrier · Coherent processing technique · B1 composite signal

1 Introduction

In recent years, the BDS is transitioning from the regional system (BDS-2) to the global system (BDS-3). According to the development plan of the BDS, the BDS-3 satellites not only need to broadcast a new interoperable signal B1C and a new authorized service signal B1A, but also have to be backward compatible with legacy BDS-2 B1I signal. Since the central frequencies of the regional system B1I signal and the global system B1 signal are not the same, the new modulation technique needs to be applied in the BDS B1 band to achieve multi-frequency multiplexing and backward compatibility.

© The Editor(s) (if applicable) and The Author(s), under exclusive license to Springer Nature Singapore Pte Ltd. 2020
J. Sun et al. (Eds.): CSNC 2020, LNEE 650, pp. 537–550, 2020.
https://doi.org/10.1007/978-981-15-3707-3_51

In addition, due to the constant envelope constraint and the asymmetric spectrum in the B1 band, the new multicarrier constant-envelope multiplexing technique also needs to be introduced.

These system constraints have promoted the emergence of new modulation and multiplexing techniques. More specifically, the SCBOC modulation [1] and CEMIC multiplexing [2, 3] techniques are adopted in the BDS-3 B1 band to construct a multicarrier constant-envelope composite navigation signal. In particular, the SCBOC modulation technique is introduced into the B1I signal to move its main energy from the global system B1 frequency to the regional system B1 frequency. In addition, the CEMIC multiplexing technique combines all the useful signals in the B1 band into a wideband constant-envelope composite signal by introducing additional intermodulation terms. However, as of now, the SCBOC modulation has only been regarded as a means to achieve the smooth update of the BDS, whose high-precision ranging potential has not been fully understood and utilized. Since the single-sideband complex subcarrier introduced in the BDS-3 B1I signal has a high frequency, it is not difficult to predict that the SCBOC modulation will bring great ranging performance potential. However, at the same time, the SCBOC modulated signal also introduces many new tracking challenges.

The first challenge is the well-known tracking ambiguity threat. Similar to other BOC-class modulated signals, the auto-correlation function (ACF) of the SCBOC modulated signal has multiple side peaks, which means that it is possible to track the side peaks instead of the main peak. Since the modulation order of the global system B1I signal is large, the ambiguity threat in this situation is very serious. In addition, different from the binary phase shift keying (BPSK) and other BOC-class modulated signals, the ACF of the SCBOC modulated signal is a complex function. Such a complex correlation peak cannot be tracked by traditional receivers [4]. When the subcarrier phase of the local replica is not aligned with that of the received signal, the energy moves from the real part to the imaginary part, which will cause the estimation deviation of the carrier phase, and vice versa. The coupling relationship between the carrier phase and the subcarrier phase makes it difficult to process the SCBOC modulated signal. One possible solution is the BPSK-Like method [5], but it ignores the ranging performance potential brought by the high-frequency subcarrier. Other existing unambiguous tracking methods [6–10] can only deal with the case where the correlation function is a real function, and cannot be applied to the SCBOC modulated signals. These complex tracking challenges and difficulties prevent the exploiting of the ranging potential of the SCBOC modulated signal.

To solve these problems, this paper proposes a high-precision coherent processing technique, which makes full use of the coherence between B1I and B1C signals. The proposed algorithm can not only exploit the ranging performance brought by high-frequency complex subcarriers without loss, but also greatly simplify the implementation complexity of the receiver. The stable carrier estimation result of the B1C signal is used to help recover the carrier of the B1I signal, while the high-precision delay estimation result of the B1I signal is used to help track the delay of the code and subcarrier of the B1C signal. The experimental results of live BDS-3 signals verify the effectiveness and correctness of the proposed algorithm. This paper provides a new solution for the high-precision application of the BDS B1 composite signal and has great reference value for receiver designers.

2 Problem Description

This section is mainly divided into two parts. The first one introduces the system constraints in the BDS B1 band and the B1 composite signal model. The second part analyses the ranging performance potential and tracking challenges brought by the single-sideband complex subcarrier.

2.1 System Constraints and Signal Model

There exist many system constraints in the signal design of the BDS-3 B1 band. Figure 1 shows the spectrum constraints of the BDS-3 B1 band. As can be seen from Fig. 1, on the one hand, the BDS-3 satellites have to broadcast the legacy BDS-2 B1I signal at the frequency of $f_{B1I} = 1561.098$ MHz to meet the constraint of backward compatibility. On the other hand, the BDS-3 satellites need to broadcast a new interoperable signal B1C at the frequency of $f_{B1} = 1575.42$ MHz to meet the constraints of compatibility and interoperability between GNSSs. In addition, the new authorized service signal B1A is also broadcast at f_{B1} to meet the performance growth needs of advanced users. Finally, these useful baseband signals in the same band need to be multiplexed into a wideband constant-envelope composite navigation signal to meet the constraint of the constant envelope.

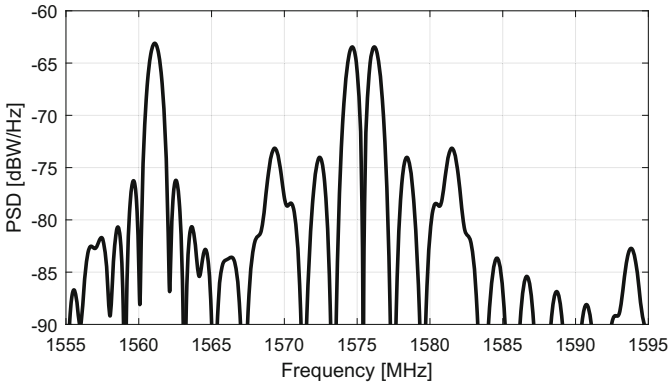

Fig. 1. The spectrum constraint of BDS-3 B1 band

These system constraints have promoted the emergence of new modulation and multiplexing techniques. More specifically, the SCBOC modulation and CEMIC multiplexing techniques are adopted in the BDS-3 B1 band to construct a multicarrier constant-envelope composite navigation signal. In particular, the SCBOC modulation

technique is introduced into the B1I signal to move its main energy from the global system B1 frequency to the regional system B1 frequency. In addition, the CEMIC multiplexing technique combines all the useful signals in the B1 band into a wideband constant-envelope composite signal by introducing additional intermodulation terms. Therefore, the B1 wideband composite signal broadcast by BDS-3 satellites can be modeled as

$$S_{\mathrm{B1}}(t) = \mathrm{Re}\left\{\left(\sqrt{P_{\mathrm{B1I}}}\mathrm{e}^{\mathrm{j}\phi_{\mathrm{B1I}}}s_{\mathrm{B1I}}(t) + \sqrt{P_{B1C}}\mathrm{e}^{\mathrm{j}\phi_{B1C}}s_{B1C}(t) + \sqrt{P_{B1A}}\mathrm{e}^{\mathrm{j}\phi_{B1A}}s_{B1A}(t) + I_{IM}(t)\right)\mathrm{e}^{\mathrm{j}2\pi f_{B1}t}\right\} \tag{1}$$

where P_i, ϕ_i, and $s_i(t)$ are the nominal power, initial phase, and baseband complex envelope of the corresponding signal component $i = B1I, B1C, B1A$, respectively. The initial phases ϕ_{B1I} and ϕ_{B1C} are equal, and the baseband complex envelope can be further given by

$$s_{B1I}(t) = d_{B1I}(t)c_{B1I}(t)\gamma_{sc}(t) \tag{2}$$

$$s_{B1C}(t) = \frac{1}{2}d_{B1C}(t)c_{B1C-d}(t)sc_a(t) + c_{B1C-p}(t)\left[\sqrt{\frac{1}{11}}sc_b(t) + \mathrm{j}\cdot\sqrt{\frac{29}{33}}sc_a(t)\right] \tag{3}$$

where $d_{B1I}(t)$ and $d_{B1C}(t)$ are the navigation messages of B1I and B1C signal, respectively. $c_{B1I}(t)$, $c_{B1C-d}(t)$, and $c_{B1C-p}(t)$ are the ranging codes of the B1I signal, data channel, and pilot channel of B1C signal, respectively.

$sc_a(t) = \mathrm{sign}\left(\sin\left(2\pi f_{sc,a}t\right)\right)$ and $sc_b(t) = \mathrm{sign}\left(\sin\left(2\pi f_{sc,b}t\right)\right)$ are the sine-phased square wave subcarriers with subcarrier frequency $f_{sc,a} = 1f_0$ and $f_{sc,a} = 6f_0$ used by the narrowband BOC(1,1) component and the wideband BOC(6,1) component, respectively, where $f_0 = 1.023$ MHz is the GNSS baseline frequency. In addition,

$$\gamma_{sc}(t) = \mathrm{sign}\left(\cos\left(2\pi f_{sc,B1I}t\right)\right) - \mathrm{j}\cdot\mathrm{sign}\left(\sin\left(2\pi f_{sc,B1I}t\right)\right) \tag{4}$$

is the single-sideband complex subcarrier with the frequency of $f_{sc,B1I} = f_{B1} - f_{B1I} = 14f_0$, where $\mathrm{sign}(x)$ is the sign function which takes value of 1 for $x \geq 0$ and -1 for $x < 0$. $I_{IM}(t)$ is the additional intermodulation term to maintain the constancy of the composite signal envelope.

Considering the effect of the bandlimiting filter, the single-sideband complex subcarrier $\gamma_{sc}(t)$ can be approximated as $\gamma_{sc}(t) \approx \mathrm{e}^{-\mathrm{j}2\pi f_{sc,B1I}t}$. Ignoring the influences of the authorized service signal and the introduced intermodulation terms, Using (1)–(4), the received B1 wideband composite signal at the antenna of the GNSS receiver can be represented as

$$
\begin{aligned}
r_{B1}(t) = & \underbrace{\sqrt{P_{B1I}} d_{B1I}(t-\tau) c_{B1I}(t-\tau) \cos\left(2\pi\left(f_{B1} - f_{sc,B1I} + f_D\right)t + \varphi + 2\pi f_{sc,B1I}\tau\right)}_{r_{B1I}(t)} \\
& + \underbrace{\frac{1}{2}\sqrt{P_{B1C}} d_{B1C}(t-\tau) c_{B1C-d}(t-\tau) sc_a(t-\tau) \cos(2\pi(f_{B1} + f_D)t + \varphi)}_{r_{B1C-d}(t)} \\
& + \underbrace{\sqrt{\frac{P_{B1C}}{11}} c_{B1C-p}(t-\tau) sc_b(t-\tau) \cos(2\pi(f_{B1} + f_D)t + \varphi)}_{r_{B1C-pb}(t)} \\
& - \underbrace{\sqrt{\frac{29P_{B1C}}{33}} c_{B1C-p}(t-\tau) sc_a(t-\tau) \sin(2\pi(f_{B1} + f_D)t + \varphi)}_{r_{B1C-pa}(t)} \\
& + n(t)
\end{aligned}
\tag{5}
$$

where τ is the signal propagation delay, f_D is the Doppler shift, φ is the carrier phase, $n(t)$ is the zero-mean Gaussian white noise with PSD N_0. The Eq. (5) is the B1I and B1C signal model to be processed.

2.2 Ranging Potential and Tracking Challenges

The previous subsection gives the model of the BDS B1 composite signal. It can be seen from (5) that the BDS-3 B1I signal using SCBOC(14,2) modulation can be easily processed by the traditional BDS-2 receiver as a legacy BPSK(2) modulated signal, which meets the requirement of backward compatibility. However, as of now, the SCBOC modulation has only been regarded as a means to achieve the smooth update of the BDS, whose high-precision ranging potential has not been fully understood and utilized. Therefore, this paper, for the first time, points out that the $r_{B1I}(t)$ in Eq. (5) can not only meet the constraint of the backward compatibility but also contain great ranging performance potential. To fully use it will probably improve the ranging and positioning precision of the BDS-3 B1 band.

Figure 2 shows the Gabor bandwidth comparison of all civil signals in GNSS community. Generally, the wider the Gabor bandwidth, the better the thermal noise performance, which means the potential of signal in ranging and positioning performance is greater. As can be seen from Fig. 2, the SCBOC(14,2) modulated signal and the AltBOC(15,10) modulated signal have the first-class Gabor bandwidths of all civil signals, which means that they have great ranging performance potential. In addition, compared with the AltBOC(15,10) modualted signal, which has similar Gabor bandwidth, the SCBOC(14,2) modulated signal requires a narrower front-end bandwidth to receive the entire main lobe, which means receiving and processing SCBOC(14,2) modulated signal has a better cost performance. To sum up, the SCBOC(14,2) modulated signal has great ranging potential, and its effective use is worthy of attention. However, at the same time, the SCBOC modulated signal also introduces many new tracking challenges.

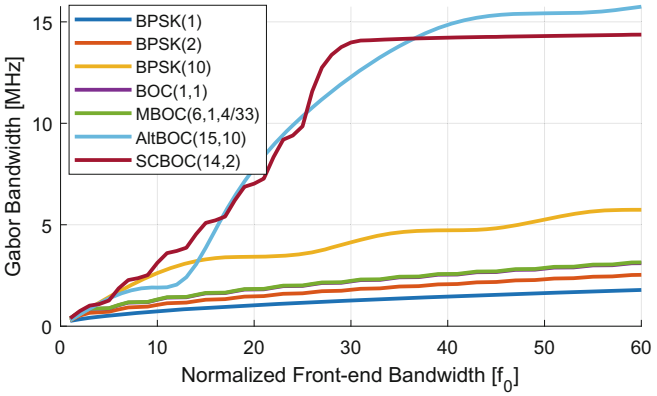

Fig. 2. The Gabor bandwidth comparison of all civil signals in GNSS community

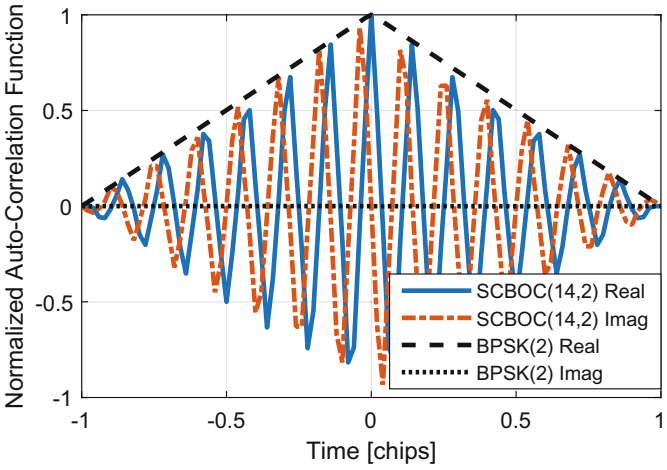

Fig. 3. Normalized auto-correlation function of the SCBOC(14,2) modulated signal

Figure 3 shows the normalized ACF of the SCBOC(14,2) modulated signal. For comparison, the ACF of the BPSK(2) modulated signal is also given. As can be seen from Fig. 3, on the one hand, the ACF of the SCBOC (14,2) modulated signal has multiple side peaks, which means that it is possible to track the side peaks instead of the main peak. This is the well-known ambiguity threat in BOC-class modulated signals. Since the modulation order of the SCBOC(14,2) is large, the ambiguity threat in this situation is very serious. On the other hand, different from the ACF of BPSK and BOC-class modulated signals, the ACF of SCBOC(14,2) modulation signal is a complex function. Such a complex correlation peak cannot be tracked by traditional receivers. When the subcarrier phase of the local replica is not aligned with that of the received signal, the energy moves from the real part to the imaginary part, which will cause the estimation deviation of the carrier phase, and vice versa. The coupling relationship

between the carrier phase and the subcarrier phase makes it difficult to process the SCBOC modulated signal. These complex tracking challenges and difficulties prevent the exploiting of the ranging potential of the SCBOC modulated signal.

3 Proposed Algorithm

This section makes full use of the coherence between B1I and B1C signals to solve these tracking challenges while pursing the ranging potential brought by the high-frequency complex subcarrier. More specifically, we propose a high-precision coherent processing technique. The proposed algorithm can not only exploit the ranging performance brought by high-frequency complex subcarriers without loss, but also greatly simplify the implementation complexity of the receiver. The stable carrier estimation result of the B1C signal is used to help recover the carrier of the B1I signal, while the high-precision delay estimation result of the B1I signal is used to help track the delay of the code and subcarrier of the B1C signal. Therefore, using the coherence between B1I and B1C signals, only the prompt correlators are required in the tracking phase of the B1C signal, thus greatly simplifying the implementation complexity of the receiver while exploiting the high-precision ranging performance.

Figure 4 shows the schematic representation of the coherent processing technique for BDS B1I and B1C signals. It should be noted that a coherent discriminator is adopted in subcarrier branch. Colors help identify different loops. The carrier loop is in red, the code loop is in green, and the subcarrier branch is in blue. For the sake of simplicity, all signals in Fig. 4 are complex signals.

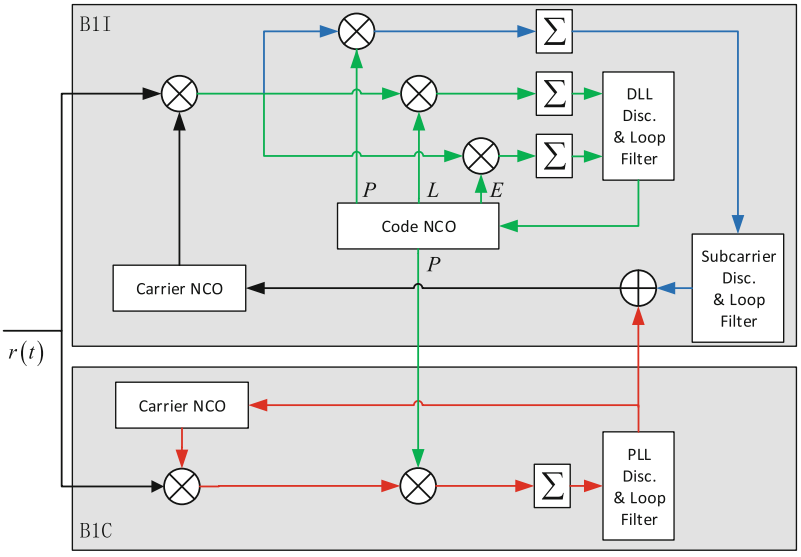

Fig. 4. Schematic representation of the coherent processing technique for BDS B1I and B1C signals (coherent discriminator used by subcarrier branch), carrier loop (red), code loop (green), subcarrier branch (blue)

At first, the carrier of the B1C signal can be removed from the received B1 composite signal by multiplying locally generated complex carrier $y_{\mathrm{B1C}}(t) = \mathrm{e}^{-\mathrm{j}\left(2\pi\left(f_{B1}+\hat{f}_D\right)t+\hat{\varphi}+\pi/2\right)}$, where $\hat{f}_D$ and $\hat{\varphi}$ are the estimations of Doppler shift and carrier phase, respectively. Note that only B1C pilot narrowband BOC(1,1) component is considered here. $\pi/2$ represents that the B1I and B1C pilot BOC(1,1) component are phase-orthogonal. Similarly, the carrier of the global system B1I signal can be removed from the received B1 composite signal by multiplying locally generated complex carrier $y_{SCBOC}(t) = \mathrm{e}^{-\mathrm{j}\left(2\pi\left(f_{B1}-\hat{f}_{sc,B1I}+\hat{f}_D\right)t+\hat{\varphi}+\hat{\varphi}_{sc,B1I}\right)}$, where $\hat{f}_{sc,B1I}$ is the estimation of the subcarrier frequency, and $\hat{\varphi}_{sc,B1I} = 2\pi\hat{f}_{sc,B1I}\hat{\tau}_s$ is the estimation of the subcarrier phase, and $\hat{\tau}_s$ is the phase delay estimation in the subcarrier dimension.

Then, the product of the locally generated code with the received signal is subjected to the coherent integration to calculate the correlators output results. For the SCBOC (14,2) modulated signal, the early (E), prompt (P), and late (L) correlators output results are needed and can be represented as

$$\begin{aligned} P_{SCBOC} &= \frac{1}{T}\int_0^T r_{\mathrm{B1}}(t)\cdot y_{\mathrm{SCBOC}}(t)\cdot c_{\mathrm{B1I}}(t-\hat{\tau}_c)\cdot \mathrm{d}t \\ E_{SCBOC} &= \frac{1}{T}\int_0^T r_{\mathrm{B1}}(t)\cdot y_{\mathrm{SCBOC}}(t)\cdot c_{\mathrm{B1I}}(t-\hat{\tau}_c-\Delta_c/2)\cdot \mathrm{d}t \\ L_{SCBOC} &= \frac{1}{T}\int_0^T r_{\mathrm{B1}}(t)\cdot y_{\mathrm{SCBOC}}(t)\cdot c_{\mathrm{B1I}}(t-\hat{\tau}_c+\Delta_c/2)\cdot \mathrm{d}t \end{aligned} \tag{6}$$

where T is the coherent integration time, $\hat{\tau}_c$ is the phase delay estimation in code dimension, Δ_c is the spacing between E and L replicas for the code discriminator.

Using the coherence between B1I and B1C signals, the delay estimation of the code and subcarrier of the B1C signal can be recovered by that of the B1I signal. Therefore, for the B1C signal, only the P correlators output are required and can be represented as

$$P_{B1C} = \frac{1}{T}\int_0^T r_{B1}(t)\cdot y_{B1C}(t)\cdot C_{B1C\_pilot}(t-\hat{\tau}_c)\mathrm{sign}\left(\sin\left(2\pi f_{sc,B1C\_a}(t-\hat{\tau}_c)\right)\right)\cdot dt \tag{7}$$

Therefore, the corresponding correlators output can be given by

$$\begin{aligned} P_{B1C} &= \sqrt{2P_{B1C}}R_{B1C}(\tau-\hat{\tau}_c)\,\mathrm{sinc}(\Delta f_D T)\mathrm{e}^{\mathrm{j}(\pi\Delta f_D T+\Delta\varphi)} \\ P_{SCBOC} &= d\sqrt{2P_{B1I}}R_{B1I}(\tau-\hat{\tau}_c)\,\mathrm{sinc}\left(\left(\Delta f_D-\Delta f_{sc,B1I}\right)T\right)\mathrm{e}^{\mathrm{j}\left(\pi\left(\Delta f_D-\Delta f_{sc,B1I}\right)T+\Delta\varphi+2\pi f_{sc,B1I}\tau-2\pi\hat{f}_{sc,B1I}\hat{\tau}_s\right)} \\ E_{SCBOC} &= d\sqrt{2P_{B1I}}R_{B1I}(\tau-\hat{\tau}_c-\Delta_c/2)\,\mathrm{sinc}\left(\left(\Delta f_D-\Delta f_{sc,B1I}\right)T\right)\mathrm{e}^{\mathrm{j}\left(\pi\left(\Delta f_D-\Delta f_{sc,B1I}\right)T+\Delta\varphi+2\pi f_{sc,B1I}\tau-2\pi\hat{f}_{sc,B1I}\hat{\tau}_s\right)} \\ L_{SCBOC} &= d\sqrt{2P_{B1I}}R_{B1I}(\tau-\hat{\tau}_c+\Delta_c/2)\,\mathrm{sinc}\left(\left(\Delta f_D-\Delta f_{sc,B1I}\right)T\right)\mathrm{e}^{\mathrm{j}\left(\pi\left(\Delta f_D-\Delta f_{sc,B1I}\right)T+\Delta\varphi+2\pi f_{sc,B1I}\tau-2\pi\hat{f}_{sc,B1I}\hat{\tau}_s\right)} \end{aligned} \tag{8}$$

where $R_{B1C}(\tau-\hat{\tau}_c)$ is the ACF of the B1C pilot BOC(1,1) component, $R_{B1I}(\tau-\hat{\tau}_c)$ is the code dimension ACF of the SCBOC(14,2) modulated signal, $\Delta f_D = f_D - \hat{f}_D$ and $\Delta\varphi = \varphi - \hat{\varphi}$ are the corresponding estimation errors, respectively. $\Delta f_{sc,B1I} = f_{sc,B1I} -$

$\hat{f}_{sc,B1I}$ is the subcarrier frequency estimation error, $2\pi\left(f_{sc,B1I}\tau - \hat{f}_{sc,B1I}\hat{\tau}_s\right) = \Delta\varphi_{sc,B1I}$ is the subcarrier phase estimation error.

By assuming the perfect Doppler shift and subcarrier frequency synchronization, that is, $\Delta f_D \approx 0$ and $\Delta f_{sc,B1I} \approx 0$, the correlators outputs (8) can be further simplified as

$$\begin{aligned}
P_{B1C} &= \sqrt{2P_{B1C}}R_{B1C}(\tau - \hat{\tau}_c)\mathrm{e}^{\mathrm{j}(\Delta\varphi)} \\
P_{SCBOC} &= d\sqrt{2P_{B1I}}R_{B1I}(\tau - \hat{\tau}_c)\mathrm{e}^{\mathrm{j}\left(\Delta\varphi + 2\pi f_{sc,B1I}\tau - 2\pi\hat{f}_{sc,B1I}\hat{\tau}_s\right)} \\
E_{SCBOC} &= d\sqrt{2P_{B1I}}R_{B1I}(\tau - \hat{\tau}_c - \Delta_c/2)\mathrm{e}^{\mathrm{j}\left(\Delta\varphi + 2\pi f_{sc,B1I}\tau - 2\pi\hat{f}_{sc,B1I}\hat{\tau}_s\right)} \\
L_{SCBOC} &= d\sqrt{2P_{B1I}}R_{B1I}(\tau - \hat{\tau}_c + \Delta_c/2)\mathrm{e}^{\mathrm{j}\left(\Delta\varphi + 2\pi f_{sc,B1I}\tau - 2\pi\hat{f}_{sc,B1I}\hat{\tau}_s\right)}
\end{aligned} \tag{9}$$

Then, the correlator outputs are input to the discriminators to get the estimation error. Considering the code loop uses a standard DLL to process E_{SCBOC} and L_{SCBOC} correlator outputs, detailed DLL operations are not discussed further. Similarly, the carrier loop uses a standard PLL to process P_{B1C} correlator outputs, so the PLL operations are not discussed further. The following discussion focuses on the operation of the subcarrier branch.

From (9), it is possible to design discriminators of subcarrier branch. Generally, there are two classes of discriminators can be employed. The first class is coherent discriminators, in which the effect of the residual carrier phase is neglected ($\Delta\varphi = 0$), while the other class is non-coherent discriminators, which are designed to operate even in the presence of the residual carrier phase errors ($\Delta\varphi \neq 0$). For the coherent discriminators, an example can be

$$\phi_{c,SCBOC}\left(\Delta\varphi_{sc,B1I}\right) = \arctan\left(\frac{\mathrm{Re}(P_{SCBOC})}{\mathrm{Im}(P_{SCBOC})}\right) \tag{10}$$

when the residual carrier phase is small enough and can be approximated as $\Delta\varphi = 0$, the P_{SCBOC} correlator results can be directly used to calculate the subcarrier phase estimation error. For the non-coherent discriminators, an example can be

$$\phi_{nc,SCBOC}\left(\Delta\varphi_{sc,B1I}\right) = \arctan\left(\frac{\mathrm{Re}\left(P_{SCBOC}P_{B1C}^{*}\right)}{\mathrm{Im}\left(P_{SCBOC}P_{B1C}^{*}\right)}\right) \tag{11}$$

where $*$ represents conjugate operator. The working principle of (11) can be verified by trigonometric identity.

Next, the filtered B1I subcarrier estimation error and the filtered B1C carrier estimation error are both input to the carrier NCO of the B1I to update the locally generated complex carrier $y_{\mathrm{SCBOC}}(t)$, thus closing the tracking loop.

When the unambiguous but low-precision code dimension delay estimation $\hat{\tau}_c$ and the high-precision but ambiguous subcarrier dimension delay estimation $\hat{\tau}_s$ are obtained, the final propagation delay estimation $\hat{\tau}$ can be represented as

$$\hat{\tau} = \hat{\tau}_s + \text{round}\left(\frac{\hat{\tau}_c - \hat{\tau}_s}{T_s}\right) \times T_s \tag{12}$$

where $T_s = 1/2f_{sc,B1I}$ is the subcarrier chip width.

4 Experimental Results

In this section, the live BDS-3 signals are used to verify the correctness and effectiveness of the proposed algorithm and further investigate the performance of the method. It should be noted that the data set used in this paper was collected on December 9, 2019, which contains valid B1 wideband composite signals since there are already 28 BDS-3 satellites in orbit.

Table 1 shows parameters used in the receiver for real data processing. The front-end central frequency is 1575.42 MHz. The front-end filter bandwidth is 40 MHz. Therefore, zero-IF complex digital signals can be obtained. The sampling frequency is 40 MHz, which is wide enough to contain the entire main lobe of the B1 composite signal. The carrier loop is achieved using a second-order frequency lock loop (FLL) aided three-order PLL. The code loop is implemented using a second-order DLL, and the subcarrier discriminator uses a coherent discriminator. The coherent integration time is constant at 1 ms, which is the length of one code period. It should be noted that the loop parameters used are typical values for land applications.

Table 1. Parameters used in the receiver for real data processing

Parameter	Value
Front-end central frequency	1575.42 MHz
Front-end filter bandwidth	40 MHz
Sampling frequency	40 MHz
Sampling type	Complex I and Q
FLL order	2
FLL bandwidth	2 Hz
PLL order	3
PLL bandwidth	20 Hz
DLL order	2
DLL bandwidth	5 Hz
DLL early-minus-late spacing	0.2 chips
Subcarrier branch order	2
Subcarrier branch bandwidth	5 Hz
Integration time	1 ms

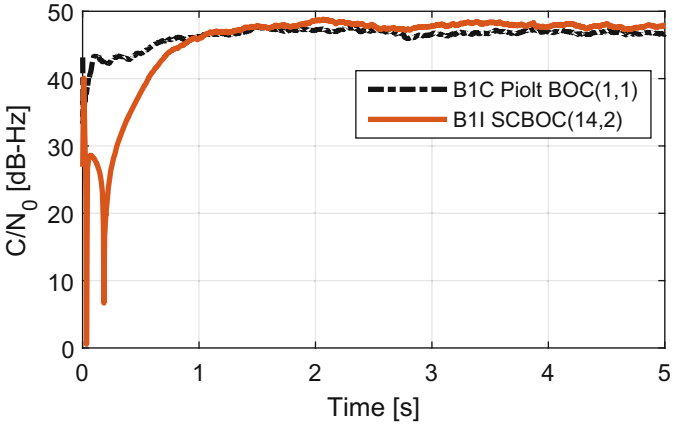

Fig. 5. C/N_0 estimation for the B1I and B1C signals

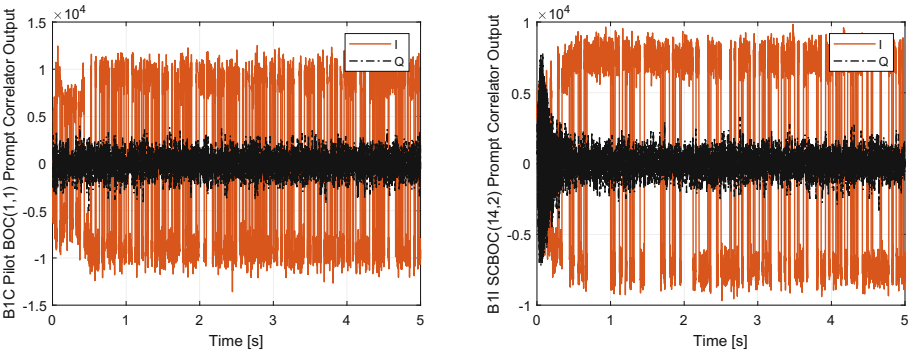

Fig. 6. Prompt correlator output results (Left: B1C pilot BOC(1,1) component. Right: B1I SCBOC(14,2) component)

Figure 5 shows the C/N_0 estimation for the B1I and B1C signals. It can be seen from Fig. 5 that after about 1 s, the C/N_0 of the proposed method tends to be stable, which means the proposed method can stably track the SCBOC(14,2) modulated signal. In addition, the proposed method takes a longer time to enter the stable tracking phase, which is because the carrier needs to be tracked stable at first and then the complex subcarrier starts to effectively demodulate.

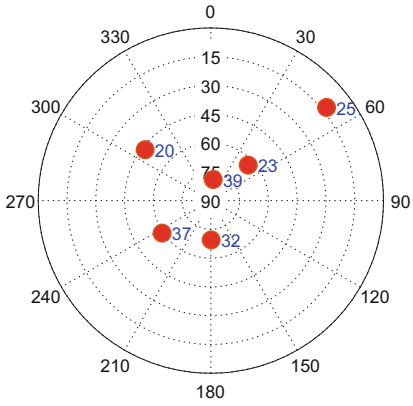

Fig. 7. The skyplot of the BDS-3 satellites

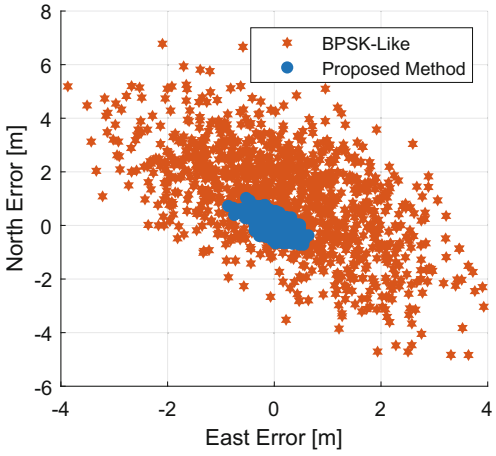

Fig. 8. The comparison of the horizontal positioning errors using proposed method and BPSK-Like technique

Figure 6 shows the prompt correlator outputs of the B1 composite signal. The left is the prompt correlator outputs of the B1C pilot BOC(1,1) component, including the in-phase (I) and quadrature (Q) parts. Comparing the amplitudes of the I and Q parts, it can be clearly seen that the main energy of the prompt correlator output is maintained in the I branch rather than the Q branch, which means the carrier of the composite signal has been perfectly tracked. In addition, it can be seen that the overlay code modulated on the B1C pilot component is also parsed in the in-phase branch. The right is the prompt correlator output of the SCBOC(14,2) component, including the I and Q parts. Similarly, it can be seen that the main energy of the prompt correlator output is retained in the I branch and the B1I navigation message can be clearly demodulated.

The above results show the measurement performance of a single channel, and the following parts analyze the positioning performance of the proposed method. The experimental time was selected at 15:14 on December 9, 2019, Beijing time. Figure 7 shows the skyplot of the BDS-3 at that time. It can be seen from Fig. 7 that there are six available BDS-3 satellites, and their PRN numbers are 20, 23, 25, 32, 37, 39, respectively. The position dilution of precision (PDOP) value is 2.73, which is enough to complete stable single-point positioning.

Figure 8 shows the comparison of the horizontal positioning errors using proposed method and BPSK-like techniques. It can be clearly seen from Fig. 8 that the proposed method has a significant positioning precision improvement due to the utilization of the high-frequency subcarrier ranging performance. In this experiment, compared with the traditional BSPK-Like reception mode, the proposed method reduces the east error from about ± 4 m to ± 1 m, and the north error is reduced from around ± 6 m to ± 1 m. It is not difficult to predict that when the number of available satellites increases, the distribution of visible satellites can be improved. At that time, the positioning performance using proposed method can be further improved, perhaps even to sub-meter positioning applications.

These results verify the correctness and effectiveness of the proposed algorithm. The experimental results show that the proposed algorithm can achieve better ranging performance and higher positioning precision. In the future, the effects of the ionosphere and the multipath on the proposed algorithm should be further analyzed.

5 Conclusions

For the single-sideband complex subcarrier introduced by the BDS-3 B1I signal to achieve the system smooth update, this paper, for the first time, points out that the single-sideband complex subcarrier can not only meet the constraint of the backward compatibility but also contain great ranging performance potential. To fully use it will greatly improve the ranging and positioning precision of the BDS-3 B1 band. However, the single-sideband complex subcarrier also introduces the serious ambiguity threat and complex coupling relationship in correlation function. These complicated tracking challenges and difficulties prevent the exploiting of the ranging potential brought by the single-sideband complex subcarrier.

To solve this problem, this paper proposes a high-precision coherent processing technique, which makes full use of the coherence between B1I and B1C signals. The proposed algorithm can not only exploit the ranging performance brought by high-frequency complex subcarriers without loss, but also greatly simplify the implementation complexity of the receiver. The experimental results of live BDS-3 signals verify the effectiveness and correctness of the proposed method. This paper provides a new solution for the high-precision application of the BDS B1 composite signal and has great reference value for receiver designers.

References

1. Yao, Z., Lu, M.: Constant envelope combination for components on different carrier frequencies with unequal power allocation. Proc. ION ITM 629–637 (2013)
2. Yao, Z., Guo, F., Ma, J., Lu, M.: Orthogonality-based generalized multicarrier constant envelope multiplexing for DSSS signals. IEEE Trans. Aerosp. Electron. Syst. **53**(4), 1685–1698 (2017)
3. Yao, Z., Lu, M.: Signal multiplexing techniques for GNSS: the principle, progress, and challenges within a uniform framework. IEEE Signal Process. Mag. **34**(5), 16–26 (2017)
4. Sleewaegen, J.-M., De Wilde, W., Hollreiser, M. (eds.): Galileo ALTBOC receiver. Proc. GNSS **2**, 3 (2004)
5. Martin, N., Leblond, V., Guillotel, G., Heiries, V. (eds.): BOC (x, y) signal acquisition techniques and performances. In: Proceedings of the 16th International Technical Meeting of the Satellite Division of the Institute of Navigation (ION GPS/GNSS 2003) (2001)
6. Fine, P. (ed.): Tracking algorithm for GPS offset carrier signals. In: 1999 Proceeding of ION National Technical Meeting, 1 (1999)
7. Ward, P.W. (ed.): A design technique to remove the correlation ambiguity in binary offset carrier (BOC) spread spectrum signals. In: 2003 Proceedings of ION 59th Annual Meeting, 6 (2003)
8. Julien, O., Macabiau, C., Cannon, M.E., Lachapelle, G.: ASPeCT: unambiguous sine-BOC (n, n) acquisition/tracking technique for navigation applications. IEEE Trans. Aerosp. Electron. Syst. **43**(1), 150–162 (2007)
9. Hodgart, M., Blunt, P., Unwin, M. (eds.): The optimal dual estimate solution for robust tracking of binary offset carrier (BOC) modulation. In: Proceeding of ION GNSS (2007)
10. Borio, D.: Double phase estimator: new unambiguous binary offset carrier tracking algorithm. IET Radar Sonar Navig. **8**(7), 729–741 (2014)